Electronic Supplementary Material (ESI) for Nanoscale.

Adhesion force spectroscopy with nanostructured colloidal probes reveals nanotopography-dependent early mechanotransductive interactions at the cell membrane level

M. Chighizola, A. Previdi, T. Dini, C. Piazzoni, C. Lenardi, P. Milani, C. Schulte* and A. Podestà*

C.I.Ma.I.Na. and Dipartimento di Fisica "Aldo Pontremoli",
Università degli Studi di Milano, via Celoria 16, 20133 Milan, Italy.

*Corresponding authors: alessandro.podesta@mi.infn.it; carsten.schulte@unimi.it

SUPPLEMENTARY INFORMATION

Contents

Supersonic Cluster Beam Deposition Apparatus (SCBD)

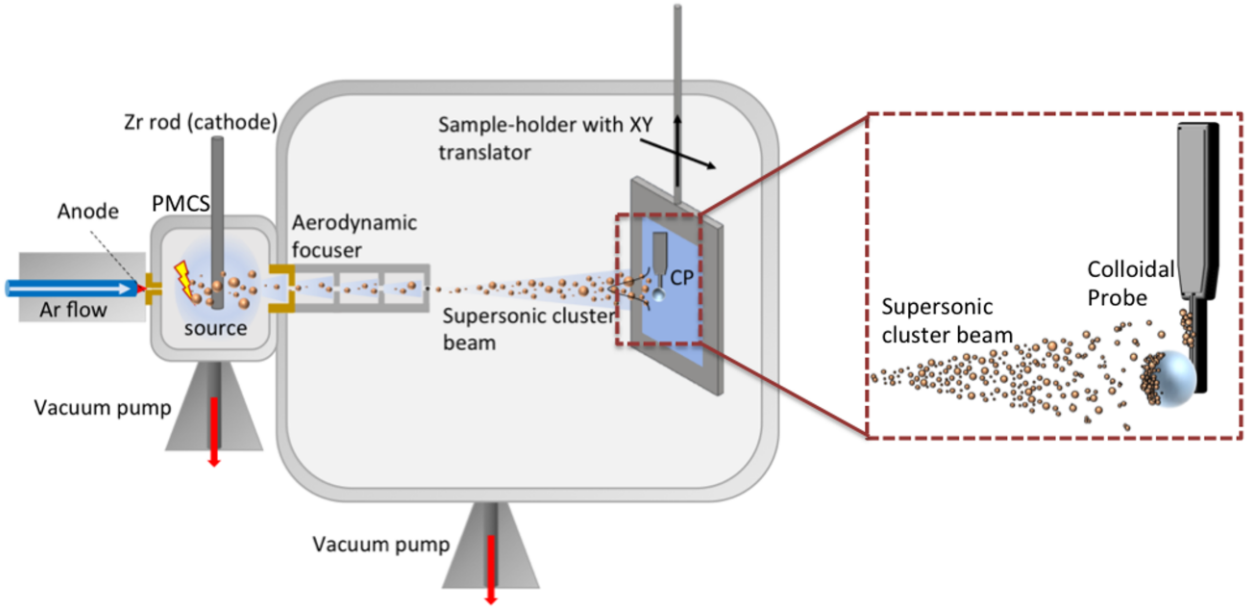

Figure S1. *A schematic representation of the SCBD apparatus that was used for the production of nt-CPs. The Zr rod is sputtered by a plasma discharge, triggered by the introduction of argon (Ar) through a pulsed valve into the source cavity and the application of a high voltage between the Zr rod and the anode. The ablated species condense into clusters and the resulting gas-clusters mixture is extracted through a nozzle and an aerodynamic focuser into a high vacuum chamber; during the process, the carrier gas-clusters mixture undergoes a supersonic expansion. The cluster beam impinges on the CP, where a thin, nanostructured* ZrO_2 *film is formed.*

Scaling of the surface roughness of ns-ZrO_2 films

To characterise the growth mechanism of ns-ZrO_2 films on colloidal probes (CPs), we dispersed the glass spheres on a flat glass microscopy slide, and deposited ns-ZrO_2 films varying the deposition times. We then imaged the coated CP surfaces by AFM in Tapping Mode (probe model: NCHV, Bruker), with relative scan speed of the tip v_{scan} = 2μm/s, and we measured the rms roughness r_q. The film thickness h was measured on the flat glass surface, in a region close to a sphere, by imaging the ns-ZrO_2 film across a sharp step produced by masking the substrate during deposition. By applying a linear regression on a loglog scale to the r_q versus h curve (see Figure S2), the value of the growth exponent b can be determined as the slope of the curve, according to the equation $r_q \sim h^b$.

According to previous results[1–3], the b parameter of the cluster-assembled ZrO_2 thin films grown on flat substrates is b = 0.368 ± 0.001 on silicon, or b = 0.31 ± 0.09 on glass coated with a monomolecular PAcrAm-*g*-(PMOXA, NH_2, Si) layer[4]. These values are compatible with the prediction of the ballistic deposition growth model (b = 0.32 - 0.25), which assumes that clusters impinge with a direction perpendicular to the plane of the substrate, and they do not diffuse significantly upon landing[5–7]. Higher values can be found when the impinging particles possess a distribution of size and different sticking probabilities.

On nt-CPs, we found b = 0.314 ± 0.017, in agreement with the value measured on flat substrates. Therefore, the curvature of the nt-CPs did not influence the growth exponent.

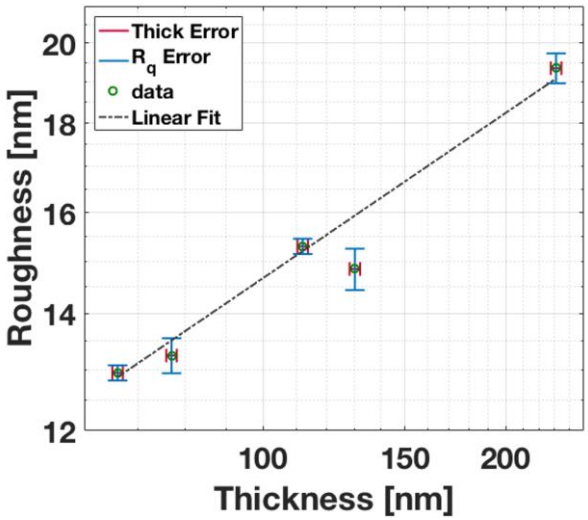

***Figure S2**. Scaling of the rms roughness r_q of ns-ZrO_2 film (i.e. roughness) on the nt-CPs.*

Mechanical stability of ns-ZrO_2 films

To test the mechanical stability of the nanostructured coating we used a stiff AFM tapping mode probe (force constant K = 50. 4 N/m) to apply high forces on the thin film, in order to record at which forces rupture events between ZrO2 nanoparticles take place.

An example of the force curve (FC) with the rupture events detected is shown in Figure S3a, while the rupture forces measured are represented in Figure S3b. Rupture forces are clustered around specific values and it is possible that the higher forces events represent cascade rupture events, where groups of nanoparticles simultaneously detach, while the lower forces represent the tip slipping across a nanoparticle, or small nanoparticles detaching from low-attachment points. The lowest rupture force detected is around F~ 70 nN, that is almost 25 times larger than the highest force measured during the force spectroscopy experiment.

Furthermore, we scanned in Tapping Mode the surface of the contact region of an nt-CP after a whole day of force spectroscopy experiments. The image obtained is shown in Figure S3c, after subtraction of the spherical curvature in order to highlight the morphological details at the nanoscale. The granularity of the surface due to the presence of the ns-ZrO2 thin film is clearly evident.

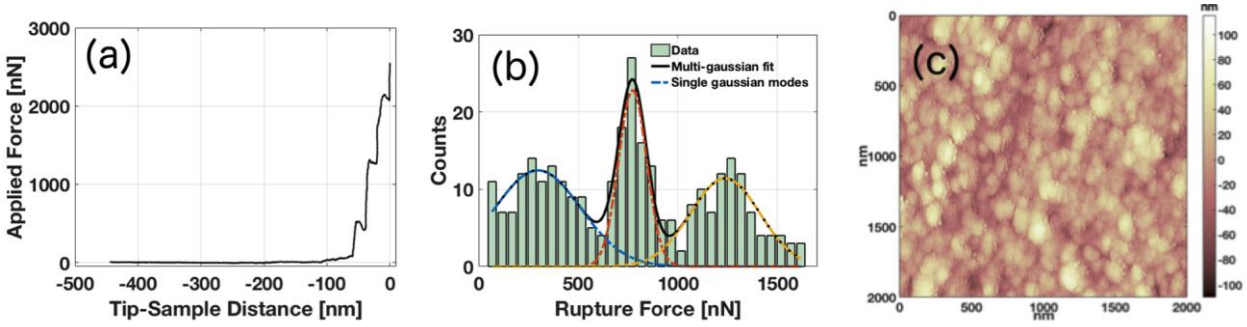

Figure S3*. (a) Representative FC with three rupture events detected; (b) distribution of the rupture event forces from all FCs, with multi-gaussian fit highlighted; (c) scan of the contact surface of a nt-CP after force spectroscopy experiment.*

Data Analysis

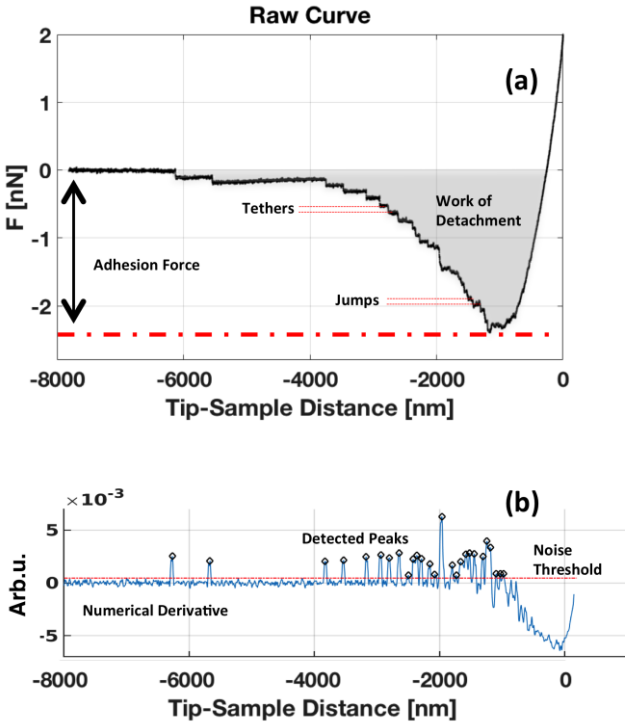

Figure S4. (a) *The retraction part of a representative FC, with the two different possible unbinding events, jumps and tethers, total adhesion force and work of detachment shown.* ***(b)*** *Numerical derivative of the FC used to identify and locate the unbinding events.*

Statistics and error analysis

For each observable ψ_{FCs} extracted by each force curve (FC) a mean value ψ_{cell} was evaluated for each cell. The error σ_{cell} associated to ψ_{cell} was obtained by summing in quadrature the standard deviation of the mean σ_{ψ} of the results coming from the single FCs and an estimated instrumental error $\sigma_{instrum}$ ($\sigma_{instrum} / \psi = 3\%$)[8]:

$$\psi_{cell} = \frac{\sum_i^n \psi_{FCs}}{n}$$

where *n* is the number of force curves per each cell,

$$\sigma_{cell} = \sqrt{\sigma_{\psi}^2 + \sigma_{instrum}^2}$$

The final mean value ψ_{mean} representative of the cell population behaviour in a given condition was evaluated as:

$$\psi_{mean} = \frac{\sum_i^n \psi_{cell}}{N}$$

where *N* is the number of cells investigated for the given condition.

The final error σ_{mean} associated to ψ_{mean} was calculated by summing in quadrature the propagated error of the mean σ_s and the standard deviation of the mean of the singles cell values ψ_{cell}:

$$\sigma_{\mathrm{mean}} = \sqrt{\sigma_{\mathrm{std}}^2 + \sigma_{\mathrm{s}}^2}$$

where

$$\sigma_{\mathrm{s}} = \frac{1}{N}\sqrt{\sum_i \sigma_{cell}^2}\,, \quad \sigma_{std} = \sqrt{\frac{\sum_i^n (\psi_{cell,i} - \psi_{fin})^2}{N}}$$

Force curves during contact

To test the stability of the Z-piezo upon contact of the CP with the sample in close-loop mode, we recorded the cantilever deflection as a function of the contact time *t*, up to *t* = 240s.

The time-dependent deflection is shown in Figure S5. On a stiff substrate, a smooth drift is observed (~10 nm in 240 s), corresponding to a maximum variation of the applied force of approximately 0.5 nN after 240s. On the cell surface, a similar drift is observed superimposed to small and slow (tens of nm in tens of seconds) fluctuations, due to the adjustment of the cell below the probe, probably accompanied by internal reorganisation of the cytoskeleton[9].

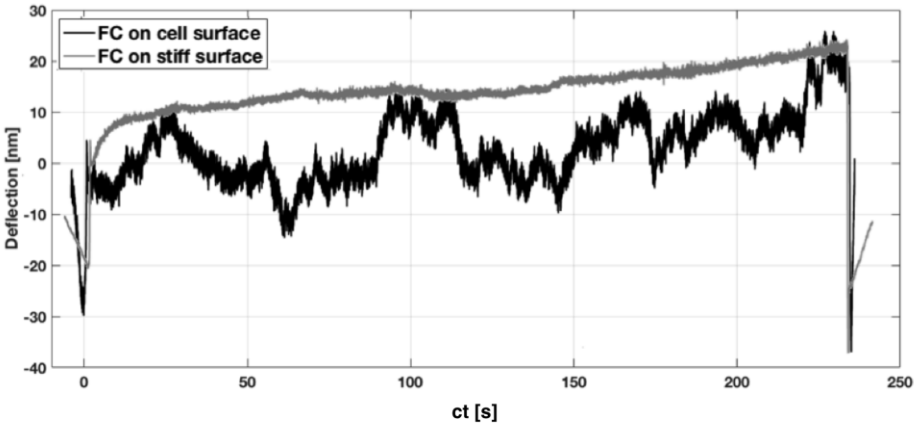

Figure S5. *Representative deflection versus contact time curves.*

Dependence of the adhesion force on the contact times, with the contribution of the tethers

The evaluation of the tether contribution to the total adhesion force F_a was evaluated as follow: for each contact time, the mean value of the tethers unbinding force has been evaluated and multiplied by the mean number of tethers N_t per FC, to obtain the tether background adhesion value.

The contribution of the tethers then has been subtracted from the adhesion force F_a, in order to calculate the contribution of the jumps. The obtained total jump adhesion force was eventually divided by the mean number of jumps N_j, in order to calculate the mean adhesion force per jump presented in Figures 4 and 5 of the main text.

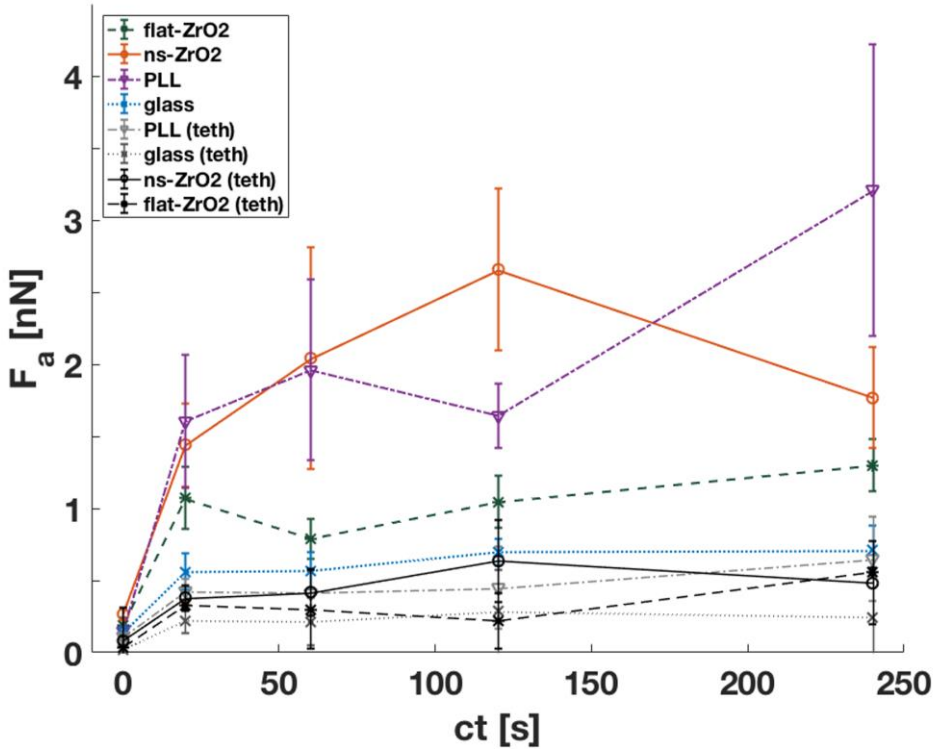

Figure S6. *Dependence of the adhesion force on the contact times as in Figure 3a; in addition, the contribution of the tethers (calculated as described above) is shown.*

Representative retraction force curves at different contact times

We show representative of FCs of the adhesive behaviour of the cells on the different surfaces for contact time *ct* =20s, 60s, 120s.

It is possible to observe the differences in the adhesion force F_a, work of detachment *W*, and number of jumps N_j, respectively. In particular, it can be seen how the adhesion on the ns-ZrO_2 surface (at ct=60 sec) reaches values compatible to the adhesion on the PLL, even in the presence of much less detachment events.

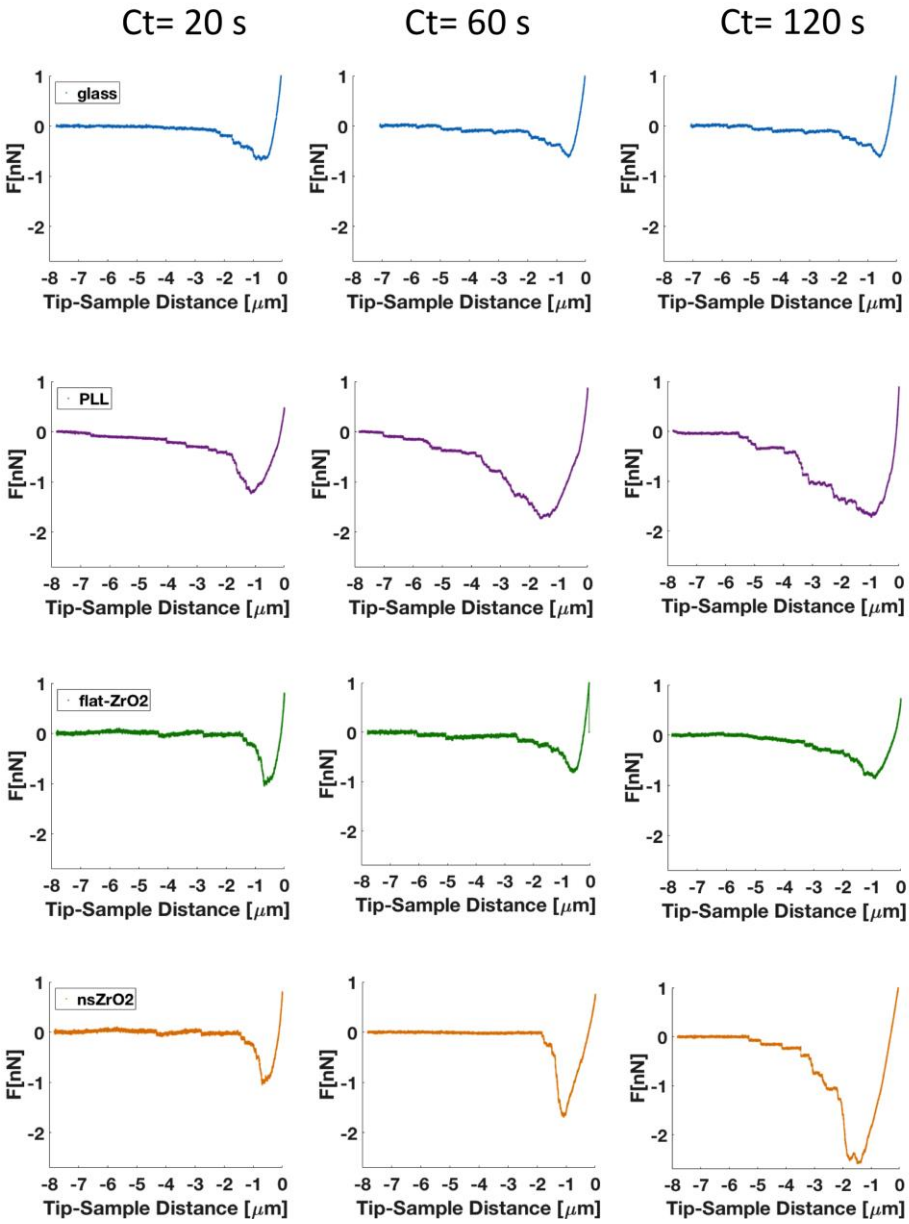

Figure S7*. Representative FCs at ct=20 s, 60 s, 120 s for each condition: glass (blue), PLL (violet), flat-ZrO_2 (green), ns-ZrO_2 (orange).*

Regarding the occurrence of jump events over a longer distance in the PLL condition, it must be pointed out that the positive charge of the PLL coating may favour on the one hand unspecific, electrostatic binding events of surface receptors, and on the other hand the polymeric nature of PLL with its long chains can unfold and be pulled away from the probe surface. This could favour detachment events occurring at higher separations, compared to the other conditions. In the PLL condition, the jump events could therefore more frequently be caused also by non-integrin surface receptors that are in some way attached to the cytoskeleton, as e.g. CD44 or syndecan-4. However, for the moment being we can only speculate about this.

Bibliography

(1) Borghi, F.; Podestà, A.; Piazzoni, C.; Milani, P. Growth Mechanism of Cluster-Assembled Surfaces: From Submonolayer to Thin-Film Regime. *Phys. Rev. Appl.* **2018**, *9* (4), 044016. https://doi.org/10.1103/PhysRevApplied.9.044016.

(2) Borghi, F.; Sogne, E.; Lenardi, C.; Podestà, A.; Merlini, M.; Ducati, C.; Milani, P. Cluster-Assembled Cubic Zirconia Films with Tunable and Stable Nanoscale Morphology against Thermal Annealing. *J. Appl. Phys.* **2016**, *120* (5), 055302. https://doi.org/10.1063/1.4960441.

(3) Podestà, A.; Borghi, F.; Indrieri, M.; Bovio, S.; Piazzoni, C.; Milani, P. Nanomanufacturing of Titania Interfaces with Controlled Structural and Functional Properties by Supersonic Cluster Beam Deposition. *J. Appl. Phys.* **2015**, *118* (23), 234309. https://doi.org/10.1063/1.4937549.

(4) Schulte, C.; Lamanna, J.; Moro, A. S.; Piazzoni, C.; Borghi, F.; Chighizola, M.; Ortoleva, S.; Racchetti, G.; Lenardi, C.; Podestà, A.; et al. Neuronal Cells Confinement by Micropatterned Cluster-Assembled Dots with Mechanotransductive Nanotopography. *ACS Biomater. Sci. Eng.* **2018**, *4* (12), 4062–4075. https://doi.org/10.1021/acsbiomaterials.8b00916.

(5) Barabási, A.-L.; Stanley, H. E. Fractal Concepts in Surface Growth by A.- L. Barabási /core/books/fractal-concepts-in-surface-growth/0D9076FC287B60B2B1126BB165112F13 (accessed Sep 4, 2019). https://doi.org/10.1017/CBO9780511599798.

(6) Family, F.; Vicsek, T. Scaling of the Active Zone in the Eden Process on Percolation Networks and the Ballistic Deposition Model. *J. Phys. Math. Gen.* **1985**, *18* (2), L75–L81. https://doi.org/10.1088/0305-4470/18/2/005.

(7) Robbins, M. O.; Cieplak, M.; Ji, H.; Koiller, B.; Martys, N. Growth in Systems with Quenched Disorder. In *Growth Patterns in Physical Sciences and Biology*; Garcia-Ruiz, J. M., Louis, E., Meakin, P., Sander, L. M., Eds.; NATO ASI Series; Springer US: Boston, MA, 1993; pp 65–75. https://doi.org/10.1007/978-1-4615-2852-4_8.

(8) Puricelli, L.; Galluzzi, M.; Schulte, C.; Podestà, A.; Milani, P. Nanomechanical and Topographical Imaging of Living Cells by Atomic Force Microscopy with Colloidal Probes. *Rev. Sci. Instrum.* **2015**, *86* (3), 033705. https://doi.org/10.1063/1.4915896.